Available online at www.sciencedirect.com

ScienceDirect

Energy Procedia 126 (201709) 501–508

Energy Procedia

www.elsevier.com/locate/procedia

72nd Conference of the Italian Thermal Machines Engineering Association, ATI2017, 6–8 September 2017, Lecce, Italy

Numerical simulation of a complete charging-discharging phase of a shell and tube thermal energy storage with phase change material

F. Fornarelli[a,*], V. Ceglie[a], B. Fortunato[a], S.M. Camporeale[a], M. Torresi[a], P. Oresta[a], A. Miliozzi[b]

[a] *Dipartimento di Meccanica, Matematica e Managment (DMMM), Politecnico di Bari, via Orabona 4, 70125 Bari, Italy*

[b] *ENEA Italian National Agency for New Technologies, Energy and Sustainable Economic Development, Casaccia Research Centre, Via Anguillarese, 301 00123 S. Maria di Galeria, Rome, Italy*

Abstract

Numerical simulations of a shell and tube energy storage device based on a phase change material (PCM) in vertical position are performed. The heat transfer fluid (HTF) is a diathermic oil and the PCM, made by molten salts, is confined within a closed shell surrounding the tube where the HTF flows. The energy loss through the external wall is included. The test has been carried out within the experimental activity performed by ENEA. A complete cycle is considered: the initial stabilization, the charging phase and the discharging phase. Details of flow behavior within the molten PCM are described highlighting its influence on the device performance.

Peer-review under responsibility of the scientific committee of the 72nd Conference of the Italian Thermal Machines Engineering Association

Keywords: Phase change material (PCM); latent heat thermal energy storage (LHTES); shell-and-tube; convection; molten salts

1. Introduction

The efficiency and flexibility requirements in the use of different energy systems introduced in the scientific community the need to develop innovative approaches. The smart grid management of energy production connects conventional energy production systems with renewable energy ones in order to maximize the efficiency. Therefore, the storage of energy represents a key point to realize these connections between different production systems. Latent heat thermal energy storage (LHTES) has a high energy density having small dimension thanks to the high thermal capacity of phase change materials (PCMs). However, the high thermal resistance of PCMs needs to be managed in

* Corresponding author. Tel.: + 39 080 5963627; fax: + 39 080 5963411
E-mail address: francesco.fornarelli@poliba.it

1876-6102
Peer-review under responsibility of the scientific committee of the 72nd Conference of the Italian Thermal Machines Engineering Association
10.1016/j.egypro.2017.08.220

order to maximize the heat transfer [1]. Several works try to study the process either experimentally or numerically. In this scenario, the optimization of the heat transfer efficiency in such device represents the objective of scientists and engineers. The use of corrugated or finned tubes in order to increase the contact surface between HTF/PCM [2, 3], the introduction of micro or nano particle in the PCM [4, 5, 6], the orientation of the device respect to the buoyancy force [7, 8, 9, 10] are several examples of the efforts that the scientific community is making in order to enhance the heat transfer in such devices. Typically, in a LHTES device the heat storage in the PCM and the heat release to the HTF are called charging and discharging, respectively. Pal and Joshi [11] studied the charging of a LHTES device characterized by a high aspect ratio placed in vertical position, but they suppose a uniform heat source. In their study they found that the natural convection plays a key role in the heat transfer especially in the first stages of melting. Recently, Muhammad et al. [12] confirmed the higher convection influence in the charging phase with respect to the discharging phase, but they restricted their evaluation to a specific case. The change of boundary condition is expected to influence the heat transfer conditions. In concentrated solar plant (CSP), the heat transfer fluid (HTF) flows within a closed circuit and it exchanges thermal energy flowing through enclosures filled with PCM. The heat flux can be positive or negative according to the presence of solar input. In the charging phase the HTF represents the heat source for the PCM and the hypothesis of uniform heat source could be not consistent with the phenomenon. For this reason, the simulation of the flow field inside the HTF could have a significant effect improving the prediction accuracy with respect simplified models. The PCM behavior can be modelled by means of the Navier-Stokes equations coupled with an enthalpy-porosity model to be able to catch the phase change as reported in several works [13, 14] where particular care should be used in the setup of the model parameters as recently confirmed by Kheirabadi & Groulx [15]. Here, following the experimental tests performed by ENEA on a LHTES devices, numerical simulations of the complete single module of the ENEA's LHTES device are made. Both, the HTF and the PCM are modelled solving the Navier-Stokes equations considering the energy equation for the heat transfer. Therefore, the heat flux between the HTF and the PCM is calculated and not modelled according to empirical correlations. Moreover, the heat loss through the insulated PCM enclosure is considered. Here, a complete charging/discharging cycle is reproduced, including stabilization. Comparison between the temperatures monitored during the experiments and the numerical results is reported and the details of the flow field within the PCM are reported and discussed.

Nomenclature

TES	Thermal energy storage
LHTES	Latent heat thermal energy storage
PCM	Phase change materials
HTF	Heat transfer fluid
CSP	Concentrated solar plant

2. PCM device

The present work is based on an experiment performed by ENEA on a Latent Heat Thermal Energy Storage (LHTES). The geometry is of a shell-and-tube type where the Heat Transfer Fluid (HTF) flows in the inner tube from the top to the bottom, whereas the external tube is filled with a material with a high heat capacity. In table 1 the HTF properties are reported considering their dependence with respect to the temperature.

The main dimensional parameters of the device are reported in tab. 2 and a schematic of the geometry under study is shown in figure 1. The device is placed in vertical position, and the HTF flows from the top down to the bottom. Here, a particular PCM is considered, whose characteristics are listed in tab. 3. The thermal dissipation of the PCM is limited by means of an isolation space filled of rock wool. The characteristics of the insulator are listed in tab. 4. Within the PCM, a thermal probe (b3) has been considered at the middle height of the PCM enclosure and at a radius equal to 21.6*mm*.

Table 1. Physical properties of the HTF fluid with respect to the temperature (in $^{\circ}C$)

Properties	Expressions	
Density	$\rho_{HTF} = 1020.62 - 0.614254 \cdot T - 0.000321 \cdot T^2$	$\left(\frac{kg}{m^3}\right)$
Specific Heat	$c_{p,HTF} = 1496.0 + 3.313 \cdot T + 0.0008970785 \cdot T^2$	$\left(\frac{J}{kg \cdot K}\right)$
Conducibility	$k_{HTF} = 0.118294 - 0.000033 \cdot T - 0.00000015 \cdot T^2$	$\left(\frac{W}{m \cdot K}\right)$
Dinamic Viscosity	$\upsilon_{HTF} = exp\left(\frac{560}{T+60} - 2.38\right)$	$(mPa \cdot s)$

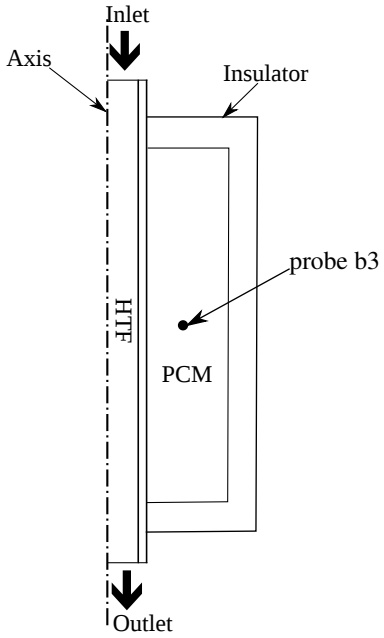

Fig. 1. Schematic of the numerical domain including, HTF duct, PCM enclosure and insulator. The position of the probe position $b3$ is also reported.

Table 2. Dimensions of the shell-and-tube geometry.

Description	Symbol	Value [mm]
External radius of the HTF duct	r_{extHTF}	8
Internal radius of the HTF duct	r_{intHTF}	7
Height of HTF duct	h_{HTF}	1097
External radius of the PCM enclosure	r_{extPCM}	35
Internal radius of the PCM enclosure	r_{intPCM}	32
Height of PCM enclosure	h_{PCM}	500

3. Numerical Model

The numerical simulations have been carried out by means of a finite volume numerical code using a 2D-axisymmetric approximation according to the problem characteristics. Two separate zones are defined in order to apply the appropriate models to simulate the HTF and PCM. The flow within the HTF has been modelled by means of the well-known single phase Navier-Stokes equations. Whereas, the PCM behaviour has been simulated by means of a solidification and melting model adding a correction term to the Navier-Stokes equations. This is able to model the phase change of the mass within the closed shell where the PCM is confined. Moreover, the Boussinesq approximation is considered in order to take into account the buoyancy effect on the liquid phase of the PCM due to the fluid density

Table 3. Physical properties of the PCM

Properties	Values	
Density	$\rho_{PCM} = 1850$	$\left(\frac{kg}{m^3}\right)$
Specific Heat	$c_{p,PCM} = 1700$	$\left(\frac{J}{kg \cdot C}\right)$
Conductivity	$k_{PCM} = 0.70$	$\left(\frac{W}{m \cdot C}\right)$
Melting Temperature	$T_{fus,PCM} = 225$	(C)
Latent Heat	$1.10 \cdot 10^5$	$\left(\frac{J}{kg}\right)$

Table 4. Physical properties of the insulator (Rock wool) and heat exchange parameters at the external wall

Properties	Values	
Density	$\rho_{rw} = 96$	$\left(\frac{kg}{m^3}\right)$
Heat Capacity	$c_{rw} = 1150$	$\left(\frac{J}{kg \cdot K}\right)$
Conductibility	$k_{rw} = 0.07$	$\left(\frac{W}{m \cdot K}\right)$
Convective Heat Exchange Coefficient	$h = 5$	$\left(\frac{W}{m^2 \cdot K}\right)$
External Temperature	$T = 298.15$	K

differences. Thus, through the energy equation, the heat exchange between different zones is taken into account. Second order accurate schemes have been considered for the spatial and temporal discretization of the equations. More details of the numerical model can be found in Fornarelli et al. [13]. Here only the governing equations for the PCM phase are reported:

$$\nabla \cdot \bar{u} = 0; \qquad \rho_0 \left(\frac{\partial \bar{u}}{\partial t} + \bar{u}\nabla\bar{u}\right) = -\nabla p + \rho\bar{g} + \bar{S} + \nabla \cdot \bar{\bar{\tau}}; \qquad \rho_0 \frac{\partial(H)}{\partial t} + \rho_0 \nabla(H\bar{u}) = \nabla(k\nabla T) \tag{1}$$

where $\nabla\bar{\bar{\tau}}$ is the viscous stress tensor. In the energy equation, the enthalpy of PCM, H, is computed as $H = h_{ref} + \int_{T_{ref}}^{T} c_p dT + \Delta H$. h is the sensible enthalpy, $\Delta H = \beta_l L$, where L is the latent heat of the PCM. Due to the Boussinesq approximation, the density change is considered only in the buoyancy term of the momentum equation where $\rho = \rho_0(1 - \beta\Delta T)$. ΔT is the difference between the actual temperature and the reference temperature, T_0, at which the reference density, ρ_0 is measured. β represents the thermal expansion coefficient of the PCM. The source term $S = \frac{(1-\beta_l)^2}{(\beta_l^3+\epsilon)} A_{mush}\vec{u}$ is introduced in the momentum equation to take into account the behaviour of the PCM during the phase change. Therefore, the S term is modulated according to the local liquid fraction β_l

$$\{\beta_l = 0 \quad if \quad T < T_{sol} \qquad \beta_l = \frac{T - T_{sol}}{T_{liq} - T_{sol}} \quad if \quad T_{sol} < T < T_{liq} \qquad \beta_l = 1 \quad if \quad T > T_{liq} \tag{2}$$

The external boundaries of the PCM are considered non-adiabatic in order to reproduce the dissipation effects of the experimental device. A simple dissipation model is considered imposing a constant temperature of the external air. The insulator zone considered in the experiment consists in an annular region that embraces the external boundary of the PCM enclosure filled with rock-wall. The characteristics of the insulator are reported in tab. 4.

4. Results

The numerical test on the heat storage device has been made with reference to the test performed by ENEA and described in the report [16]. Three phases are considered: stabilization of the temperature, charging phase and discharging phase (see fig. 2a). The comparison of the temperature time series shows a good agreement on the overall test. The maximum temperature difference between the experimental and numerical measures is about 5% and it happens during the charging phase at about 11.5h.

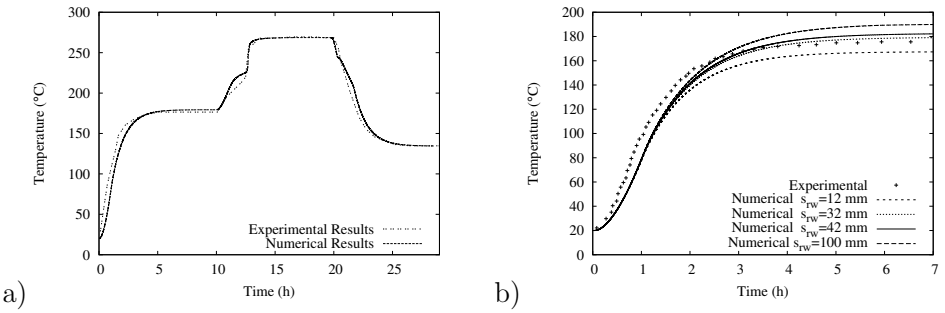

Fig. 2. Comparison of the numerical and experimental histories at probe b3. a) stabilization, charging and discharging phases; b) details of stabilization phase with reference to different thickness of insulator.

4.1. Stabilization phase

The stabilization phase consists in flowing the HTF through the circuit increasing its temperature from $20°C$ to $200°C$ with a constant ramp of $180°C/h$ and then maintaining a constant temperature. The mass flow rate is equal to $0.162kg/s$. Thus, during the pre-heating, the PCM has been maintained below its melting temperature. The heat exchange is purely conductive and the temperature histories registered in the different probe positions show the effects of the temperature increase of the HTF and the dissipation influence on the radial gradient of the temperature. Four widths of the insulator have been considered ($12mm$, $32mm$, $42mm$, and $100mm$) in order to match the experimental results. It has been necessary because of the uncertainness of the experimental setup of the insulator that influence its thermal characteristic. Therefore, the width of the insulator has been derived comparing the temperature behaviour registered at probe b3 (located in the middle radius of the PCM) during the first stabilization phase see fig.2b. The comparison shows that the insulator width that better reproduce the experimental measurements is $s = 32mm$. This insulator width has been kept constant also during charging and discharging.

4.2. Charging phase

It is well known that the thermal charge of LHTES devices represents the most critical phase of the whole thermal cycle. The numerical simulation has been carried out according to the experimental test imposing a ramp from the end of the stabilization phase. The temperature of the HTF is increased from $200°C$ to $280°C$ in $1h$ and it is kept constant until steady conditions are reached. The mass flow rate of the HTF is equal to $0.167kg/s$. The phase change affects the temperature increasing when the melting temperature is locally reached. Therefore, the convective part of the heat exchange is expected to increase its influence during the charging phase. The convective motion has been evaluated by means of instantaneous flow visualizations. In figure 3 the temperature contours within the PCM enclosure are reported. According to the numerical test the charging phase appears to be completed in about 5 hours. At the beginning of the charging phase the temperature distribution within the PCM is affected by the heat loss across the external walls. Indeed, the temperature gradient depends on the distance from the PCM walls. Thus, at the corner between the lateral and top (bottom) surfaces of the cylindrical PCM enclosure, the lowest temperature can be recognized. The effect of convective motion in the PCM is predominant in a region close to the top of the solid/liquid interface. In this zone the temperature gradient is highest and the buoyancy force trigs the formation of an annular recirculation zone. The change in slope of the temperature history registered in the probe position (b3) is analyzed against the flow visualization within the PCM in terms of temperature and pathlines. The change in slope occurs $2.6h$ after the beginning of the charging phase. The corresponding flow visualization confirms that the melting interface influences the temperature increasing as reported in fig. 4. The pathlines, within the melted PCM in the top region of the solid/liquid interface, highlight the presence of a convective motion. Whereas, in the rest of the melted PCM the flow velocities are very small, therefore the fluid tends to stratify.

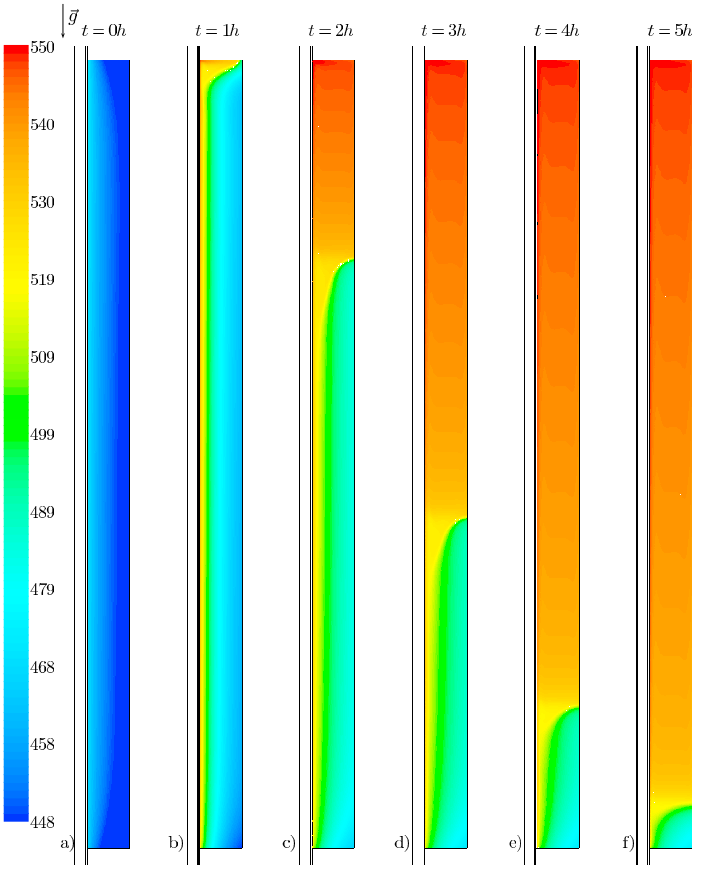

Fig. 3. Snapshots of the temperature contours during the charging phase within the PCM. The gravity vector ($\vec{g}$) is oriented from the top to the bottom. a) $t = 0h$, b) $t = 1h$, c) $t = 2h$, d) $t = 3h$, e) $t = 4h$, f) $t = 5h$, where $t = 0h$ correspond to the start of charging phase.

4.3. Discharging phase

At the end of the charging process, the discharging phase begins with a negative temperature ramp of the HTF from $280°C$ to $150°C$ in 1 hour and then maintaining the temperature constant at $150°C$. The flow rate of the HTF has been kept constant at $0.17kg/s$. Within this temperature range the solidification of the PCM occurred. Even in this case, the numerical simulation is able to give a detailed description of the PCM behavior. The probe b3 is able to distinguish exactly the start of the phase change in the PCM (see fig. 2a). The discharging time lasts about 6 hours, 1 hour more than the charging phase. The flow visualization, as reported in fig. 5, shows a slightly different behaviour of the PCM with respect to the charging process (fig. 3). Indeed, the temperature profiles appear aligned with the vertical axis of the device. The conical shape of the interface and the associated recirculation zone, described in the charging phase, does not exist anymore, justifying the longer time needed for the solidification. The discharging is more dominated by the conduction heat exchange with respect to the charging phase.

5. Conclusions

The paper reproduces an experimental test on a shell-and-tube LHTES device by means of 2D axisymmetric numerical simulation of flow equations coupled with heat transfer modelling, including the external dissipation phenomenon. The overall response of the system to the input parameters is correctly caught by the model. The monitoring of the temperature in the same probe location of the experiment gives a fairly good agreement between the present results and the experiment. The dynamics of the temperature contours during the charging phase shows a curved phase

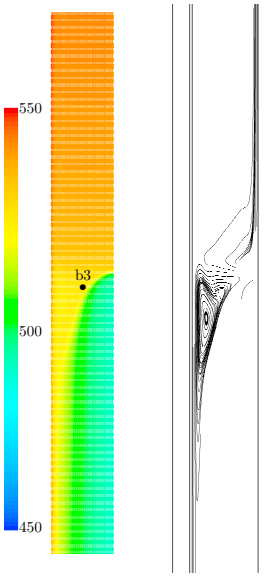

Fig. 4. On the left: Snapshots of the temperature contours during the charging phase within the PCM at $t = 2.6h$ from the start of charging phase. The black bullet represents the probe position (b3). On the right: detail of the flow recirculation zone by means of pathlines.

change interface within the PCM where a recirculation zone has been highlighted. On the other hand, during the discharging phase, the spatial distribution of the temperature within the PCM shows the absence of the convective motion described in the charging phase. These findings confirm that during the charging phase a convective contribution to the heat transfer exists but it seems to be limited by the geometrical characteristic of the LHTES device here studied.

References

[1] Liu, S. and Li, Y. and Zhang, Y., "Review on heat transfer mechanisms and characteristics in encapsulated PCMs", *Heat Transfer Engineering*, 2015, 36, 10, 880-901

[2] Languri, E.M. and Aigbotsua, C.O. and Alvarado, J.L., "Latent thermal energy storage system using phase change material in corrugated enclosures", *Applied Thermal Engineering*, 2013, 50, 1, 1008-1014.

[3] Agyenim, F. and Eames, P. and Smyth, M., "A comparison of heat transfer enhancement in a medium temperature thermal energy storage heat exchanger using fins", *Solar Energy*, 2009, 83, 9, 1509-1520.

[4] P. Oresta, F. Fornarelli and A. Prosperetti, "Multiphase Rayleigh-Bénard convection", Mechanical Engineering Reviews, Volume 1.

[5] Schmidt, L.E., Oresta, P., Toschi, F., Verzicco, R., Lohse, D., Prosperetti, A. Modification of turbulence in Rayleigh-Bnard convection by phase change (2011) New Journal of Physics, 13, art. no. 025002

[6] Sanusi, O. and Warzoha, R. and Fleischer, A.S., "Energy storage and solidification of paraffin phase change material embedded with graphite nanofibers", *International Journal of Heat and Mass Transfer*, 2011, 54, 19-20, 4429-4436.

[7] Kamkari, B. and Shokouhmand, H. and Bruno, F., "Experimental investigation of the effect of inclination angle on convection-driven melting of phase change material in a rectangular enclosure", *International Journal of Heat and Mass Transfer*, 2014, 72, 186-200.

[8] Torresi, M. and Saponaro, A. and Camporeale, S.M. and Fortunato, B., "CFD analysis of the flow through tube banks of HRSG", *Proceedings of the ASME Turbo Expo*, 2008, 7, 327-337

[9] Fornarelli, F. and Oresta, P. and Lippolis, A., "Flow patterns and heat transfer around six in-line circular cylinders at low Reynolds number", JP Journal of Heat and Mass transfer -Volume 11, Issue 1, Pages 1 - 28, Feb 2015

[10] Fornarelli, F. and Lippolis, A. and Oresta, P., "Buoyancy Effect on the Flow Pattern and the Thermal Performance of an Array of Circular Cylinders". ASME. J. Heat Transfer. 2016;139(2):022501-022501-10

[11] Pal, D. and Joshi, Y.K., "Melting in a side heated tall enclosure by a uniformly dissipating heat source",*International Journal of Heat and Mass Transfer*,2000, 44, 2, 375-387

[12] Muhammad, M.D. and Badr, O. and Yeung, H.,"CFD modeling of the charging and discharging of a shell-and-tube latent heat storage system for high-temperature applications",*Numerical Heat Transfer; Part A: Applications*, 2015, 68, 8, 813-826

[13] Fornarelli, F., Camporeale, S.M., Fortunato, B., Torresi, M., Oresta, P., Magliocchetti, L., Miliozzi, A., Santo, G. "CFD analysis of melting process in a shell-and-tube latent heat storage for concentrated solar power plants",*Applied Energy*, 164 (2016), 711-722.

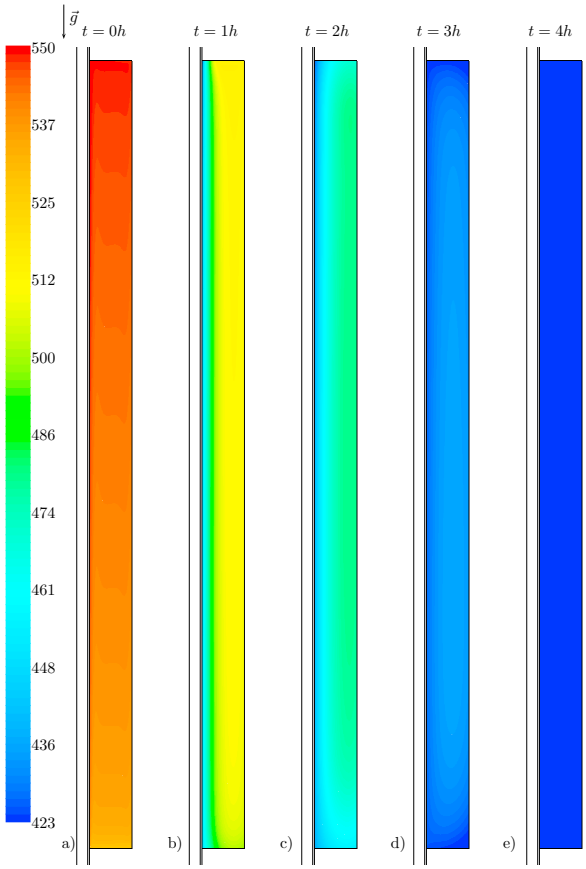

Fig. 5. Snapshots of the temperature contours during the discharging phase within the PCM. The gravity vector ($\vec{g}$) is oriented from the top to the bottom. a) $t = 0h$, b) $t = 1h$, c) $t = 2h$, d) $t = 3h$, e) $t = 4h$, where t is the time from the beginning of the discharging phase, where $t = 0h$ correspond to the start of discharging phase.

[14] Guo, S. and Li, H. and Zhao, J. and Li, X. and Yan, J., "Numerical simulation study on optimizing charging process of the direct contact mobilized thermal energy storage", *Applied Energy*, 2013, 112, 1416-1423.

[15] Kheirabadi, A.C. and Groulx, D.,"Simulating phase change heat transfer using comsol and fluent: Effect of the mushy-zone constant",*Computational Thermal Sciences*, 2015, 7, 5-6, 427-440.

[16] Miliozzi, A., Giannuzzi, G.M., Liberatore, R. "Experimental and numerical analysis of the thermodynamic behaviour of simple latent heat thermal energy storage devices" (in italian) *Energia elettrica da fonte solare Solare termodinamico (Progetto B.1.3)* Rds/Par2014/116 (2015).